Communications in Information and Systems
Volume 23, Number 1, 1–30, 2023

CATDS: cross aggregation transformer-based dynamic supplement network for underwater image enhancement

Zhixiong Huang, Jinjiang Li*, Zhen Hua, and Linwei Fan

The complex underwater environment causes light to suffer from scattering effects and wavelength-dependent attenuation, and underwater images exhibit color deviation and low contrast, which hinder the progress of related underwater tasks. Deep learning algorithms now make extensive use of multi-scale features to improve underwater image quality, but the majority of these methods do not take channel differences into account while propagating features. To this end, we propose a cross aggregation transformer (CAT), which utilizes three stages of projection-crossing-aggregation to adaptively select beneficial channels. This paper also designs a dynamic supplement underwater image enhancement network, which consists of a shallow network and an enhancement network. Through the encoder/decoder structure, the enhancement network restores the original appearance of the underwater image, while the shallow network extracts the shallow features at different scales. Both networks are designed to focus on under-enhanced regions and supplementary details in real time through the residual supplement module (RSM). The experimental findings demonstrate that CAT and RSM efficiently improve network performance and elevate the network above other advanced methods on various datasets.

1. Introduction

The resource-rich ocean promotes the vigorous development of the underwater vision, and related technologies are widely used in tasks such as marine environmental monitoring, marine resource exploration, and marine salvage.

*Research supported in part by National Natural Science Foundation of China (61772319, 62002200, 62202268 and 62272281), and the Shandong Natural Science Foundation of China (ZR2021QF134, ZR2021MF107). Contact: Jinjiang Li. Email: lijinjiang@sdtbu.edu.cn. Shandong Technology and Business University, China.

However, the complex underwater environment plays a great obstacle to underwater perception, and underwater images often show color deviation and low contrast. To improve imaging quality in underwater environment, compensating light sources are often used to create a better environment, but the captured underwater images cannot form a satisfactory illumination effect [1]. Therefore, a key area of computer vision research is how to enhance the quality of underwater images in various environments.

The atmospheric imaging model widely used in image dehazing [2, 3] also reveals the underwater degradation process. According to the Jaffe-McGlamery underwater optical imaging model [4, 5], the overall light constituting the underwater image is obtained by a linear summation of direct scattering, forward scattering, and backward scattering. Where direct scattering is the direct light from the imaging scene to the acquisition point. Both forward scattering and backward scattering are the products of refraction of light when encountering underwater suspended particles. The difference between the two is that the former comes from the imaging scene and the latter comes from other scenes, both of which result in blurred details and low contrast in underwater images [6]. In addition, unlike the atmospheric environments, the light attenuation in underwater environments is related to the propagation depth and light wavelength [7]. As the propagation depth deepens, the longer wavelengths of red and yellow light are severely lost, resulting in underwater images with predominantly green or blue color deviations. And the above problems will be aggravated with the increase of distance from the imaging scene to the acquisition point [8].

In recent years, most research has proposed a series of solutions to improve the poor-quality underwater images, which can be roughly divided into three categories: image restoration methods, image enhancement methods, and deep learning methods. The image restoration methods derive the degradation process by constructing an underwater optical imaging model, and then restore the underwater image by reversing the degradation process. Different from similar dehazing methods, most underwater methods take into account the wavelength-dependent light attenuation process to enable more accurate color restoration. Since such methods require precise estimation of parameters, the color deviation of the original image may be increased or artifacts may be introduced in the face of underwater images with various degradation levels. The introduction of artifacts will cause the color and texture of the image to be obscured, which will further damage the image clarity. The image enhancement methods enhance the visibility of underwater images by compensating the lost color and modifying the pixels in defective regions. Although such methods do not require estimation of the

imaging model, inaccurate region delineation can compromise the original appearance of the image in the face of different underwater environments and large amounts of noise.

With a large amount of image data and a complex model, the deep learning method learns how to enhance the underwater image to the target image batch by batch. To build a larger field of view, the input information is adjusted to multi-scale, multi-channel features by the encoder, and the information loss in scale changes is reduced by skip connection. However, different channels are not only diverse in content, but also in their contribution to the network. In the process of transmitting the encoder features, the skip connection transmits the beneficial and useless information to the decoder simultaneously. This direct connection makes the network pay insufficient attention to the defective regions and the visual quality of the final enhanced images suffers. Inspired by [9], this paper proposes a cross aggregation transformer and builds a dynamic supplement network for underwater image enhancement. The contributions of this paper are as follows:

1. A cross aggregation transformer (CAT) is designed. CAT adaptively selects useful contents through three processes of projection-crossing-aggregation, so that the network can focus on the contribution of different information to the resulting image.

2. We propose a dynamic supplement network consisting of two branches. The enhancement network uses the encoder/decoder structure to enhance the quality of underwater images, the shallow network extracts the shallow features of the input image. The two sub-networks focus on under-enhanced regions and supplement the detailed texture in real time through the designed residual supplement module (RSM).

3. Experiments on various public datasets show that the proposed method is superior to other advanced methods in subjective and objective aspects., and the combination of CAT and RSM brings significant gains to the network.

The remainder of this paper is organized as follows. Section 2 describes the domain related work. Section 3 introduces the modules and loss functions involved in the network. In Section 4, we first conduct an ablation study according to the relevant modules and then conduct comparative experiments with other methods. Finally, Section 5 concludes the paper.

2. Related work

2.1. Image restoration methods

Ancuti et al. [10] proposed a color channel compensation model to compensate for the loss of a specific color channel by restoring the opposition

color to zero mean. Yang et al. [11] performed retinex decomposition on the dark channel to estimate the transmission map, and used the estimated backscattered light to restore edge details, allowing effective image sharpness improvement. Berman et al. [12] considered the light attenuation in different water bodies, and introduced the color channel attenuation ratio into haze-lines model makes the underwater image restoration more comprehensive. Song et al. [13] proposed a manually annotated background light database, where the imaging model was established by the estimated background light and transmission maps, and an improved white balance algorithm was used to enhance the color and contrast. Marques and Albu [1] proposed two contrast-guided atmospheric lighting models to generate two images with prominent details and enhanced brightness for fusion. Wang et al. [14] enhanced images based on retinex theory, while the reflectance and illumination decomposition was performed after color equalization correction. Zhou et al. [15] considered underwater image segmentation and smoothing in estimating the imaging distance, eliminated backscattering with more accurate depth map, and improved image visibility with adaptive global illumination parameter. Liang et al. [16] corrected the color according to the attenuation maps of different channels, and then used a multi-scale gradient domain to repair details and remove haze. Miao et al. [17] introduced an approximate single viewpoint camera model in dealing with underwater light scattering, which effectively improved the image clarity. Zhuang et al. [18] eliminated color casts by the designed color constancy method, and then made the retinex method generate results with good visibility by applying multiorder gradient priors. Liang et al. [19] estimated the backscattered light by using hierarchical search technology, and then combined with the underwater dark channel prior to estimate the transmission map. Finally, the improved white balance method was used to further improve the image visibility. Li et al. [20] first estimated the background light by comparing the divided regions, then compensated the color of the degraded underwater image, and finally used haze-line model to remove the haze effect. Zhou et al. [21] used depth map and illuminant map to estimate backscatter and correct color, respectively, and used color compensation to eliminate red artifacts. Yan et al. [22] imitated the color constancy mechanism and horizontal cells to correct for underwater color deviation, and then used a new biological normalization model to deal with blur and noise. Li et al. [23] first compensated the attenuated color information, and then estimated the transmission map by color-line model to reverse the underwater degradation process.

2.2. Image enhancement methods

Ancuti et al. [24] respectively performed contrast enhancement and detail sharpening on the white balanced images to obtain two input, and then obtained the enhancement results through the fusion process guided by weight estimation. Azmi et al. [25] first eliminated the color cast by enhancing defect channel, then fused the two mean images to improve the contrast, and finally further enhanced the image by swarm equalization and unsharp masking technique. Awad et al. [26] fused the degraded image and the near-infrared image by measuring the contrast difference between the two, so that the detail loss due to the haze effect was compensated. Zhu et al. [27] introduced a weight map analysis in the process of fusing a series of gamma correction results, and then performed a linear saturation adjustment to further improve the image color and saturation. Zhang et al. [28] used a subinterval linear transform to process different pixel regions, and then applied contrast enhancement and detail highlighting to the low and high frequency components, respectively. Liu and Liang [29] first used color channel transfer to pre-process the image, then designed an adaptive attenuation curve to correct the color, and finally enhanced color and detail by fusing the white balance of globally guided image filtering. Zhou et al. [30] used an underwater imaging model to restore the image, where the background light was estimated from the information distribution and light scattering properties, and the projection map was obtained from the connection between luminance information and color attenuation. Zhang et al. [31] compensated the color based on the difference between color channels, then performed contrast enhancement globally and locally, and finally fused the two enhanced images and sharpened the final image. Dong et al. [32] performed color compensation and contrast enhancement in RGB color space and LAB color space, respectively, and a normalized guided filtering was introduced in the process of the contrast enhancement. Zhou et al. [33] first corrected color deviation based on self-adaptive standard deviation, and then enhanced luminance and detail through gamma correction and spatial linear adjustment. Li et al. [34] used the difference of gaussian filter and bilateral filter to separate high-frequency and low-frequency components, and performed image denoising and color correction in the two components. Zhang et al. [35] first enhanced the color and detail by a minimum color loss principle and a maximum attenuation map, then adjusted the saturation using the integral and squared integral maps, and finally further improved the visibility by balancing the difference between the A and B channels in

CLELAB space. Huang et al. [36] separate the underwater image enhancement in two steps, a manual process and a deep learning process. First, the attenuation color channel was compensated, and then the scattering and blurring were eliminated through the dual image wavelet fusion and general adaptive network.

2.3. Deep learning methods

Li et al. [37] constructed a large-scale underwater image dataset with reference images, in which the reference images are from the artificial selection results of twelve enhancement methods, and trained a baseline network for underwater image enhancement. Fu et al. [38] divided the enhancement process into two steps. First, global color compensation and local contrast enhancement were performed through a double branch network, and then the quality was further improved through compressed histogram equalization. Wang et al. [39] first combined RGB and HSV color spaces for underwater deep learning, where the former performs denoising and removing color cast, while the latter performs color, brightness, and saturation adjustments, and finally uses attention to fuse the two results. Li et al. [6] used features from RGB, HSV, and Lab color spaces to enhance images, and guided the network to focus on poor quality regions by channel attention and medium transmission. Huang et al. [40] used local binary patterns and additional detail restoration module to enhance details, and the final image was obtained by superimposing the results of both correction and restoration branching networks. Fu et al. [41] combined the UNet structure and channel normalization to process images of various underwater degradation types, allowing the network to generate cleaner enhancement results. Liu et al. [42] proposed a novel parallel attention module to focus on illumination and color features and build an adaptive learning network for underwater image enhancement. Huang et al. [43] proposed a novel adaptive group attention, which enabled the network to compress model parameters efficiently while adaptively selecting complementary visual features.

Since it is difficult to obtain corresponding air images in underwater environments, many research methods have addressed the need for paired training images by introducing generative adversarial networks (GAN). [44, 45] first introduced GAN to underwater scenes to synthesize underwater style images, so that the underwater image enhancement network was fully trained. Liu et al. [46] performed color correction of underwater images based on GAN. The network achieves a more efficient learning process by dynamically fusing global features and local features. Guo et al. [47] introduced

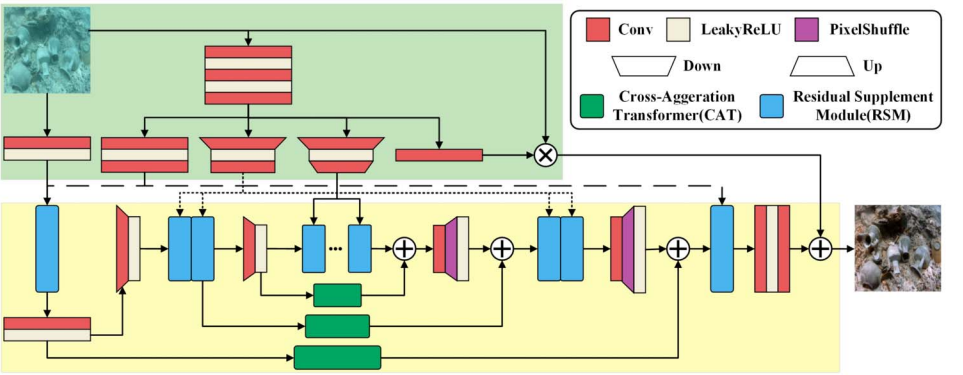

Figure 1: The main framework of the proposed network, with two trapezoids in the figure representing the decreasing and increasing image size. The overall network is mainly divided into the upper shallow network and the lower enhanced network. The structures of CAT and RSM are given in Figure 2 and Figure 3.

dense connection and residual learning in the process of underwater image enhancement using GAN, which effectively improved the reusability of features. Chen et al. [48] combined underwater image enhancement and target detection to guide the GAN to generate visually or detect more beneficial images, and combined with physical prior and deep learning to generate training datasets. Islam et al. [49] constructed a large underwater dataset containing paired and unpaired images and trained GAN based on this, where the loss of the network is calculated by the proposed perceptual loss function. Desai et al. [50] considered the effect of more attenuation factors on underwater imaging, and synthesized underwater images with the modified imaging model to train the conditional generative adversarial network. Jiang et al. [51] transformed underwater style images into air images by CycleGAN, and then improved the image clarity by encoder-decoder network.

3. Methodology

Figure 1 and algorithm 1 show the schematic figure and procedure of the proposed network, which mainly consists of a shallow network and an enhanced network. In this section, we will first introduce the main framework of the network, then elaborate on the designed CAT and RSM, and finally introduce the loss function adopted by the network.

Algorithm 1 Enhancement procedure of our method

Input: Underwater images: x

Output: Enhanced images: y

1. Extract shallow features f^s through convolution and LeakyReLU:
   $f^s = F_C(x)_{LR}$
2. Change feature scales using convolution with 2 strides and PixelShuffle:
   $f = F_C(f^s)_{LR}$
   $f = F_{PS}(F_C(f^s))_{LR}$
3. Complement details by RSM before and after scale change:
   $f = F_{RSM}(f, f^s)$
4. Input encoding features f^e into CAT and combine with decoding featuresf^d:
   $f = F_{CAT}(f_e) + f_d$
5. Use shallow features and original inputs to further enhance the color:
   $y = F_C(f)_{LR} + x \times f^s$

3.1. Network structure

The input of the proposed network is a single underwater image. It can be seen that in addition to the serious color deviation, the underwater image also has the problems of blurred details or insufficient exposure, and the brightness and contrast are also variable in different regions. Due to the layered features brought by different scales, the network can focus on specific positions, so as to carry out more thorough image enhancement. Therefore, the enhanced network adopts a network architecture similar to UNET. First, the input image is expanded from 3 channels to 64 channels by convolutional layers and LeakyReLU activation function. Then, the encoder progressively maps the input features to low-scale, high-dimensional features, while the decoder reconstructs the high-dimensional features into an enhanced image, where the features are scaled down and up through the convolutional layer with 2 strides and PixelShuffle, respectively.

In the process of scale change, the content information of features is mapped to different channels, which also means that the contribution of channels is different. For underwater image enhancement, regions of poor quality need to receive more attention. However, traditional UNet tends to use only simple skip connection to connect the same level features between the encoder and the decoder. The network does not focus on defective regions due to ignoring the variability of feature channels. Inspired by [9], we design a CAT for the skip connection, where the features before scale change in the encoder will be transmitted to the CAT, and then they are transmitted to the decoder after cross-learning. The CAT can enrich the representation

of features and obtain more accurate enhancement performance by cross-learning correlations between channels.

Due to the lack of attention to the original input information, the network can not completely correct the color deviation, and will lose some original image details. Therefore, we designed a shallow network. The underwater image first passes through a channel expansion block consisting of a convolutional layer-activation function crossover, with the number of channels expanded from 3 to 64. Corresponding to the three scales of enhanced features in the network, the features pass through three scale change blocks, respectively, where the scale change of the image is completed by a convolutional layer with 2 strides. The extracted shallow features are then transferred to each RSM. As the smaller the scale, the greater the information loss, we set 2, 4, and 8 RSM at different scales to assist the network in building more accurate colors and textures by progressively enhancing the complement of shallow features. In addition, we add a weight estimation process to the end of the shallow network to distinguish the different region contributions of the original image I_i to the final enhancement effect. We combine the estimation results with the output I_e of the enhancement network to obtain the final enhanced image I_o. The process is as follows:

$$I_o = \theta\left(I_i\right) \cdot I_i + I_e, \tag{1}$$

where $\theta\left(\cdot\right)$ represents the convolution layer, which is used to restore the expanded channel to the original channel. By introducing weight estimates for different regions, the network will pay more attention to the poorly enhanced regions, allowing for a more thorough correction of color deviation in underwater images.

3.2. Cross aggregation transformer

In the network, the input image is mapped to high-dimensional features through multiple convolutions, and the feature channels are expanded several times. However, diverse channels contribute differently to the network. When connecting the coding and decoding features at the same level, a large amount of useless information and noisy information from the encoding process are also synchronously propagated, and this undesirable information is amplified step by step in the decoder. For such problems, channel attention (CA) [52, 53] provides a solution to how to select beneficial channels. However, existing CA measures the salience of channels by convolutional layers, and the expansion of the perceptual field gradually suppresses the local

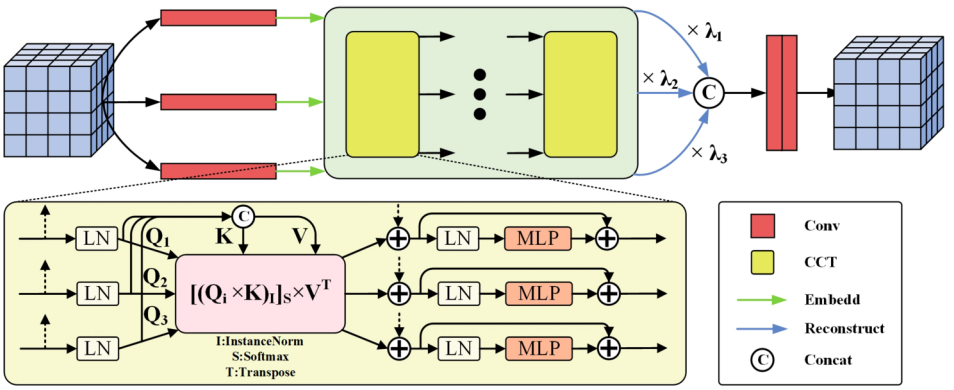

Figure 2: The specific structure of CAT, where $\lambda_1, \lambda_2, \lambda_3$ represents three learnable parameters.

modeling ability. For this reason, we propose a cross aggregation transformer (CAT), which differs from CA in that the CAT adaptively selects beneficial channels through the remote dependency building capability in the transformer.

The specific structure of CAT is shown in Figure 2. CAT is divided into three stages: projection-crossing-aggregation. First, we choose to enrich the feature representation by three convolutional layers, where the kernel size of each layer is 1*1. Thus the feature is mapped to a channel sequence, and the shape is changed from H*W to C. The three convolutional layers obtain a group of 3*C mapping features by amplifying the diversity. Then we reshape the features into flattened 2D facet sequences and perform position labeling respectively. Second, we put the three tokens into Channel-wise Cross Attention (CCA) to compute the inter-channel dependencies. Unlike [9], our main purpose is not to narrow the semantic gap, but to select more meaningful channels among the features. Therefore, the input tokens do not have scale differences. Through the Linear and LayerNorm layers, the three tokens are converted into queries $q_i (i = 0, 1, 2)$, while the key and value are from the aggregation of the three queries $k, v = \sum_{i=0}^{2} q_i$. Thereby obtaining the following CCA calculation:

$$CCA_i = [(q_i \cdot k)_I]_S \cdot v^T, \tag{2}$$

where $(\cdot)_I$ represents the instance normalization of the normalized similarity matrix, $(\cdot)_S$ represents the sigmoid function for calculating the weight, and $(\cdot)^T$ represents transpose. The three groups of channel sequences are used to

obtain correlations between channels by interactive learning of aggregated sequences, and the importance of channels is further captured by normalization and activation functions. Next, the output of the second stage is obtained by the following calculation:

$$o_i = MLP\left(q_i + CCA_i\right)_{LN} + CCA_i \tag{3}$$

In the third stage, we aggregate the outputs of the three paths. For further selection of features on different paths, three learnable parameters $\lambda_1, \lambda_2, \lambda_3$ are set to adjust the intensity of each path:

$$o = \lambda_1 o_1 + \lambda_2 o_2 + \lambda_3 o_3 \tag{4}$$

Finally, the aggregated features are recovered to the input channel by a layer of 1*1 and a layer of 3*3 convolution, and we input the aggregated features to the same level features of the decoder, so as to give the network a clearer perception of the saliency of different regions.

3.3. Residual supplement module

While the network corrects the color of underwater images, loss of detail and color deviation will affect the final quality of the image. To solve these two problems, the original input is fed to the shallow network to extract shallow features. However, simple cascaded peer features introduce supplementary information while introducing useless information. Therefore, we design a residual supplement module (RSM) to provide distillation mechanism and residual supplement for shallow features and enhanced features.

Figure 3 illustrates the structure of RSM. We first transform the shallow features f_s into a weight matrix by 1*1 convolution and Softmax activation function, and multiply them with the convolved enhanced features f_e to obtain the global feature dependencies. Next, we performed two residual connections in RSM using f_s and f_e. The first connection ensures the gradient flow of the network, and the second connection can attach the learned global dependencies to each position of the original feature. In addition, a few connection processes can reduce the computational cost of the network. The whole process is as follows:

$$f_{RSM} = W\left(\left(f_s\right)_S \times f_e + f_s\right) + f_e, \tag{5}$$

where f_e and f_s represent enhanced features and shallow features, respectively. $(\cdot)_S$ and W represent the softmax function and the weight learned by

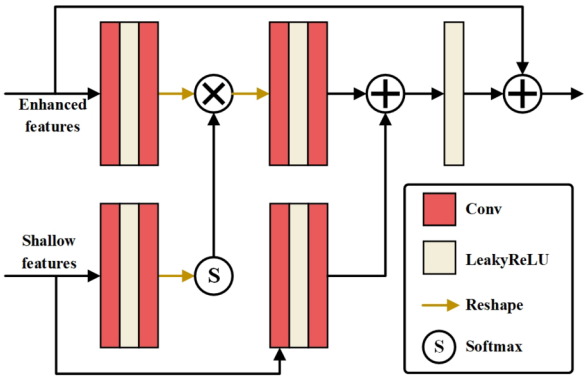

Figure 3: The structure of RSM, wherein the supplementary features are from the shallow network.

convolution. Through the application of RSM, the network will make full use of different shallow features, so as to obtain better color and texture images.

3.4. Loss function

By calculating the loss between the enhancement result and the ground truth, the end-to-end training of the proposed network is effectively supervised, and the final loss $\mathcal{L}$ of the network is obtained by combining two kinds of losses:

$$\mathcal{L} = \ell_{\text{char}}(x, y) + \mu \times \ell_{ssim}(x, y), \tag{6}$$

where x is the enhanced image, y is the ground truth, and ℓ_{char} represents the charbonnier loss, ℓ_{ssim} represents the SSIM loss. We set $\mu = 0.5$ to balance the two losses. The ℓ_{char} , which is used to measure the pixel similarity between two images, is calculated as follows:

$$\ell_{\text{char}}(x, y) = \sqrt{\|x - y\|^2 + \varepsilon^2}, \tag{7}$$

where constant ε is set to 10^{-3} to stabilize the loss. ℓ_{ssim} is used to measure the structural similarity between two images, and its definition is as follows:

$$\text{SSIM}(x, y) = \frac{(2\mu_x\mu_y + c_1)}{(\mu_x^2 + {\mu_y}^2 + c_1)} \cdot \frac{(2\sigma_x\sigma_y + c_2)}{({\sigma_x}^2 + {\sigma_y}^2 + c_2)}, \tag{8}$$

$$\ell_{s\,\mathrm{sim}}(x, y) = 1 - \mathrm{SSIM}(x, y), \tag{9}$$

where μ represents the brightness, σ represents the contrast and structure. We set $c_1 = 0.0001$ and $c_2 = 0.0009$. When the final loss $\mathcal{L}$ decreases, the pixel and structure between the enhanced results and the ground truth are closer.

4. Experiment

This section first describes the experimental setup, second conducts an ablation study to demonstrate the effectiveness of the components, and third compares with other methods on reference and non-reference datasets.

4.1. Experimental details

Datasets: After years of development, various datasets have been proposed in the field of underwater image enhancement for training and evaluation. In this paper, we used the UIEB [37] dataset for training the proposed model. The original underwater images of UIEB were obtained from multiple sources, and multiple enhancement methods were used to obtain the corresponding high-quality images. Finally, the corresponding ground truth was voted by volunteers from the multiple enhancement results. We divided the total number of 890 image pairs into 790 training pairs and 100 test pairs. In addition, the reference-free dataset EUVP [49] (130 images), ImageNet [54] (1813 images), LNRUD [55] (500 images), and UFO [56] (120 images) were also used to evaluate all methods in this paper.

Metrics: In this paper, four reference metrics (PSNR, SSIM, FSIM [57], and LPIPS [58]) and three non-reference metrics (UCIQE [59], FDUM [60], and Entropy) were used to evaluate the objective performance of the enhancement results. For the reference dataset, we used all metrics for evaluation, and for the non-reference datasets, we used the three non-reference metrics for evaluation.

Methods: We compared the proposed network with many advanced underwater image enhancement methods, including three traditional methods (CBF [24], BR [18], and ACDC [31]), two unsupervised methods (M-GAN [46] and F-GAN [49]), and three supervised methods (WaterNet [37], UIE^2-Net [39], and SCNet [41]).

Settings: We built the model using the PyTorch framework and trained it on a TITAN RTX graphics card. Since the proposed network is end-to-end, no additional pre-training is required. The total number of batches trained was 100. The learning rate was initially $2*10^{-4}$ and continuously adjusted by the Adam optimizer. In addition, all images were cropped to 256*256.

Table 1: Module configuration of each group in ablation study

	CAT	RSM
OriNet	×	×
-w/o CAT	×	√
-w/o RSM	√	×
Ours	√	√

4.2. Ablation study

As shown in Table 1, we configured four networks based on the proposed modules, and compared them on the UIEB test dataset to verify the effectiveness of the two module combinations. Figure 4 and Figure 5 show the subjective and residual comparison of all configuration, respectively, while Table 2 indicates the objective metrics for all the results. As shown in Figure 4, it can be seen that OriNet generates images with large dark regions, and the color texture of the images is also affected. Therefore, the residual

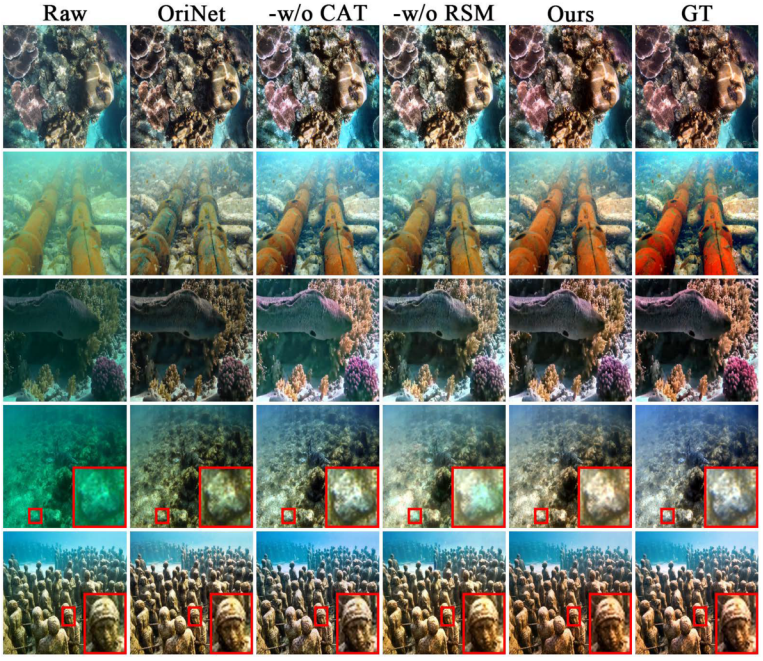

Figure 4: Visual comparison of network results with different configurations on UIEB dataset.

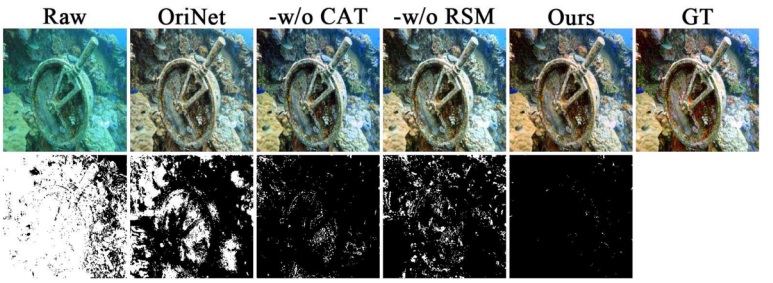

Figure 5: Residual comparison between network results and ground truth for different configurations. The white region in the residual figures represent the difference with the ground truth.

Table 2: Module configuration of each group in ablation study (**optimal**, suboptimal)

	PSNR	SSIM	FSIM	LPIPS	UCIQE	FDUM	Entropy
OriNet	22.130	0.9129	0.9550	0.1699	0.5797	0.7636	7.5525
-w/o CAT	26.062	0.9455	0.9630	0.1111	0.6156	0.8550	7.7299
-w/o RSM	25.212	0.9390	0.9619	0.1366	0.6203	0.8208	**7.7420**
Ours	**26.656**	**0.9482**	**0.9661**	**0.1098**	**0.6274**	**0.8620**	7.7382

figure of OriNet has the widest white areas, which means that the variability between the result and the ground truth is the greatest. −w/o CAT does not completely restore the color texture of the results due to the lack of CAT that focuses on the important content, and the overall exposure phenomenon is appears. −w/o RSM does not completely remove color deviation, and image clarity is affected by fogging effects. The network with the full component not only completely corrects for color deviation, but also has the best color and sharpness. The fewest white regions in Figure 5 also verify the fit of the enhanced result to the ground truth. In Table 2, the complete network achieves the best values for four reference and two non-reference metrics, while slightly underperforming the −w/o RSM on Entropy, which still demonstrates the gainfulness of using both modules.

4.3. Experiments on reference dataset

On the UIEB test dataset, we conducted reference comparisons with other advanced methods. Figure 6 and Figure 7 show the enhancement results for all methods. As can be seen in Figure 6 (a), CBF and BR introduce other

Figure 6: Visual comparison of all methods on UIEB dataset.

color effects, which corrupt the overall image color. The results of ACDC and WaterNet are dark in brightness, and ACDC shows severe color loss problem. Therefore, the four methods have the most extensive white regions in Figure 7, which represents the difference between the four enhancement results and the ground truth. The enhancement results of M-GAN, F-GAN, and SCNet have good contrast improvement and are more consistent with the ground truth color, but still fail to address the color deviation of fish. UIE^2-Net and our method can effectively enhance the contrast and clarity of the image while removing the underwater color deviation. In Figure 6 (b) and (c), CBF and ACDC results are dull in color and the original texture details are not clear. BR overcompensates the red channel, so its enhanced

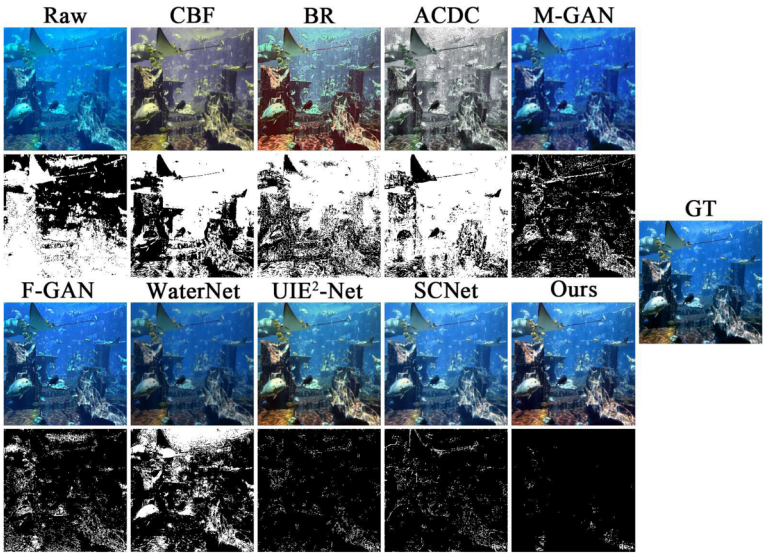

Figure 7: Residual comparison of all methods on UIEB dataset. The white region in the residual figures represent the difference with the ground truth.

images show most red artifacts. M-GAN, F-GAN, and SCNet failed to ensure the image quality improvement, and the hazing effect is deepened in some images instead. Compared with other methods, our method results in a powerful enhancement of the color, sharpness, and contrast of the images, which is related to the fact that the network focuses on different contents in various ways. By adding CAT, the deep network pays attention to the beneficial information, thus making the enhancement of underwater images better. In addition, with the increasing number of RSM as the scale changes, the features of the two branches are complemented in real time, allowing a more comprehensive recovery of color and texture in the defective regions. Therefore, our method has the least white regions in the residual figure in Figure 7, which means that our method is more similar to the ground truth.

Table 3 shows the objective performance, model parameter and FLOPs of all methods on the UIEB test dataset. Our method achieves five optimal values and two suboptimal values on the four referenced and three non-reference metrics, respectively. The comparison of the metrics in the table shows that our method is objectively closest to the ground truth, and is outstanding in terms of color, sharpness, and content richness. UIE^2-Net achieves suboptimal values for most metrics and outperforms our method in LPIPS, which is related to its good color recovery and detail enhancement.

Table 3: Metrics performance of all methods on UIEB dataset (**optimal**, suboptimal)

	PSNR	SSIM	FSIM	LPIPS	UCIQE	FDUM	Entropy	Param (M)	FLOPs (G)
CBF[24]	21.915	0.9146	0.9484	0.2163	0.5639	0.6900	7.4570	-	-
BR[18]	21.050	0.8515	0.9025	0.2708	0.5933	**0.8860**	7.7103	-	-
ACDC[31]	18.951	0.8084	0.8901	0.3442	0.5544	0.6197	7.7005	-	-
M-GAN [46]	18.720	0.6595	0.8191	0.5093	0.5356	0.4277	7.3182	45.79	14.80
F-GAN [49]	20.856	0.8267	0.9140	0.2366	0.5567	0.6320	7.4639	7.01	**10.23**
Water-Net[37]	20.477	0.8489	0.9213	0.1467	0.5685	0.6349	7.4112	1.09	142.9
UIE^2-Net[39]	26.148	0.9412	0.9636	**0.1052**	0.6210	0.7823	7.6986	**0.51**	24.2
SCNet[41]	24.731	0.9163	0.9488	0.1344	0.5916	0.7054	7.5899	0.77	21.93
Ours	**26.656**	**0.9482**	**0.9661**	0.1098	**0.6274**	0.8620	**7.7382**	11.02	34.84

BR, on the other hand, outperforms us in FDUM due to its bright color performance. In terms of model parameter and FLOPs, UIE^2-Net and F-GAN perform well, and our method does not perform well, which is a drawback of our method.

4.4. Experiments on non-reference datasets

In this paper, we also compare with other methods on several non-reference datasets. Figure 8–Figure 11 shows the effect and enlarged comparison of all methods on EUVP, ImageNet, LNRUD, and UFO datasets, respectively, while Table 4–Table 7 show the metric performance of all methods.

In Figure 8(a), M-GAN, F-GAN, SCNet, and our method restore the image appearance, while SCNet and our method have brighter colors. Comparing the details in (b), it can see that CBF, M-GAN, F-GAN, and WaterNet fail to enhance the brightness of the image, and the color texture of the fish is covered by darkness. The enhanced results of BR and ACDC are overall white, with weak color texture contrast. UIE^2-Net, SCNet and our method generate results with attractive colors, while our method is better in saturation and contrast.

As can be seen in Figure 9, BR, M-GAN, F-GAN, WaterNet, and SCNet fail to restore the original image, and their results still have varying degrees of blue and green deviation. BR also introduces the effect of red artifacts.

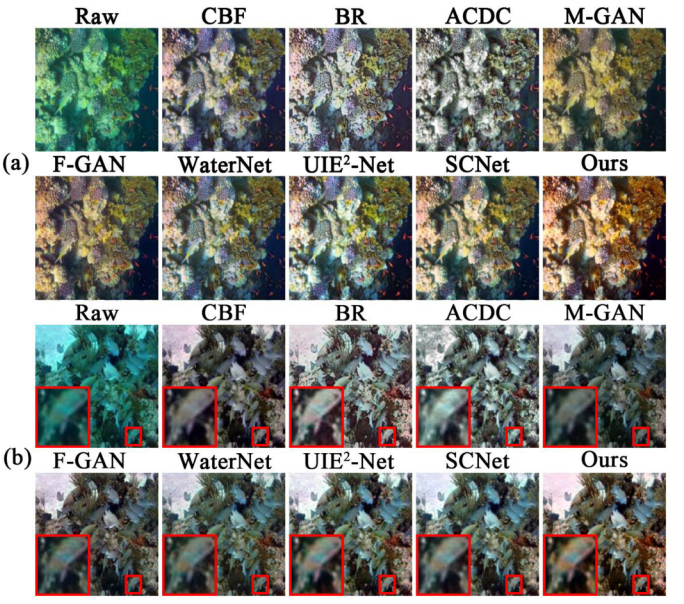

Figure 8: Visual comparison of all methods on EUVP dataset.

The results of CBF and ACDC have grayish colors, and blurred texture details of the scene in the field. UIE^2-Net and our method are much better at recovering the image colors, and the texture details are much clearer in the enlargement.

The outstanding color of our method is well illustrated in Figure 10 and Figure 11. In the visual comparison of all methods, our method effectively removes the hazing effect and exhibits bright contrast and sharpness enhancement. In the enlarged detail, the color benefits of our method are more clearly contrasted, and the more vibrant colors further improve the attractiveness of the image.

In the metric tables corresponding to the four datasets, our method achieves the best values for all UCIQE, FDUM, and most of the Entropy metrics, indicating that the enhancement results of our method have excellent color, contrast, and sharpness performance. BR outperforms our method for Entropy on the UFO dataset and achieves all sub-optimal values for FDUM, due to its excellent red channel compensation, but the frequent red artifacts affect the visibility of the resulting images.

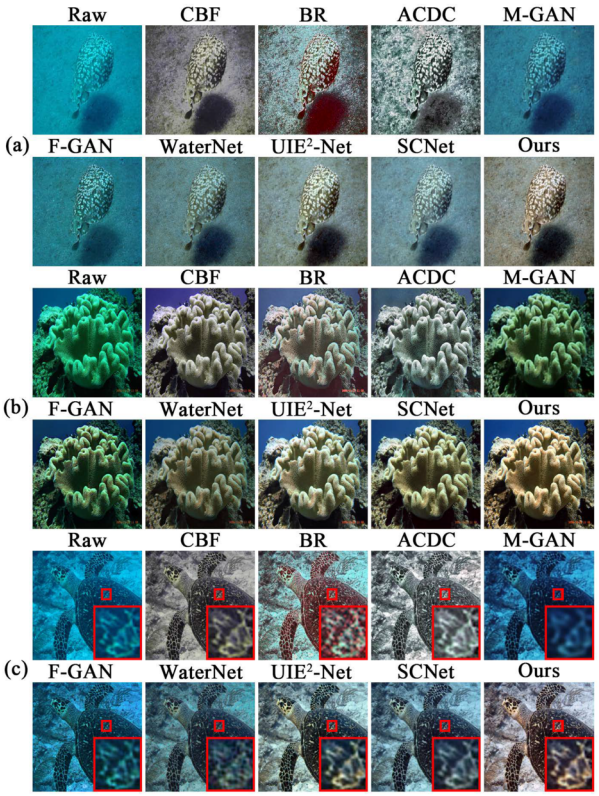

Figure 9: Visual comparison of all methods on ImageNet dataset.

4.5. Other applications

To test the enhancement effect of the proposed network in other scenes, we apply the model of this paper to the low-light dataset (DICM [61] and LIME [62]) and the overexposure dataset (MIT [63]), respectively. As shown in Figure 12, our method significantly improves the luminance of the low-light images, and the texture details covered by darkness are well recovered. The lost saturation is effectively enhanced in the overexposure scene, and the overexposed image becomes vividly colored as well as layered. The good application in both scenes further demonstrates the visibility enhancement of our method in different scenes.

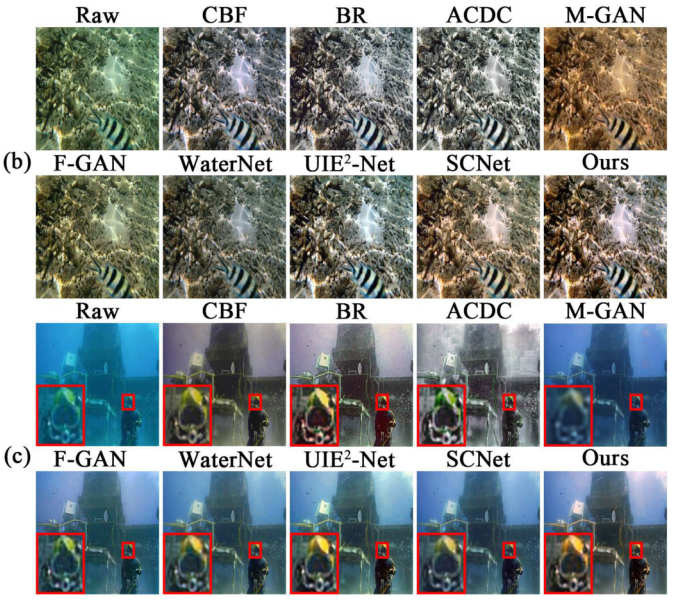

Figure 10: Visual comparison of all methods on LNRUD dataset.

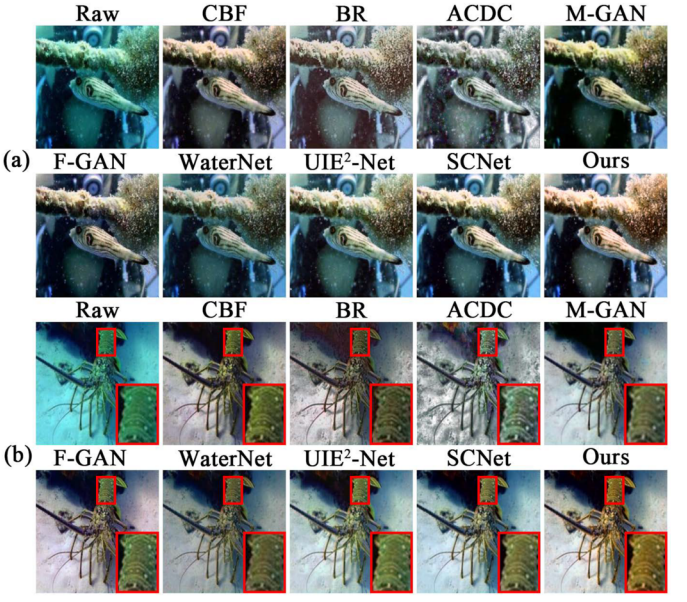

Figure 11: Visual comparison of all methods on UFO dataset.

Table 4: Metrics performance of all methods on EUVP dataset (**optimal**, suboptimal)

	UCIQE	FDUM	Entropy
CBF[24]	0.5782	0.5097	7.5711
BR[18]	0.5890	0.6293	7.7633
ACDC[31]	0.5605	0.4510	7.7558
M-GAN[46]	0.5802	0.4734	7.4852
F-GAN[49]	0.5895	0.5585	7.5276
WaterNet[37]	0.5870	0.5440	7.5125
UIE^2-Net[39]	0.6233	0.5972	7.7105
SCNet[41]	0.6127	0.5778	7.6987
Ours	**0.6380**	**0.6436**	**7.7649**

Table 5: Metrics performance of all methods on ImageNet dataset (**optimal**, suboptimal)

	UCIQE	FDUM	Entropy
CBF[24]	0.5791	0.6450	7.5354
BR[18]	0.5826	0.7520	7.6826
ACDC[31]	0.5614	0.5820	7.7097
M-GAN[46]	0.5687	0.4770	7.3713
F-GAN[49]	0.5786	0.6482	7.4722
WaterNet[37]	0.5681	0.5897	7.3939
UIE^2-Net[39]	0.6119	0.6930	7.6536
SCNet[41]	0.5995	0.6608	7.6089
Ours	**0.6269**	**0.7835**	**7.7139**

Table 6: Metrics performance of all methods on LNRUD dataset (**optimal**, suboptimal)

	UCIQE	FDUM	Entropy
CBF[24]	0.5788	0.5492	7.5359
BR[18]	0.5871	0.6696	7.7252
ACDC[31]	0.5620	0.4940	7.7341
M-GAN[46]	0.5727	0.4629	7.4310
F-GAN[49]	0.5856	0.5735	7.5141
WaterNet[37]	0.5843	0.5521	7.4705
UIE^2-Net[39]	0.6215	0.6248	7.6911
SCNet[41]	0.6111	0.6023	7.6676
Ours	**0.6354**	**0.6834**	**7.7482**

Table 7: Metrics performance of all methods on UFO dataset (**optimal**, suboptimal)

	UCIQE	FDUM	Entropy
CBF[24]	0.5901	0.5434	7.5676
BR[18]	0.5918	0.6394	**7.7517**
ACDC[31]	0.5664	0.4784	7.7325
M-GAN[46]	0.5890	0.4990	7.4146
F-GAN[49]	0.5961	0.5835	7.4804
WaterNet[37]	0.5913	0.5580	7.4930
UIE^2-Net[39]	0.6219	0.6050	7.6618
SCNet[41]	0.6196	0.6052	7.6465
Ours	**0.6362**	**0.6558**	7.7248

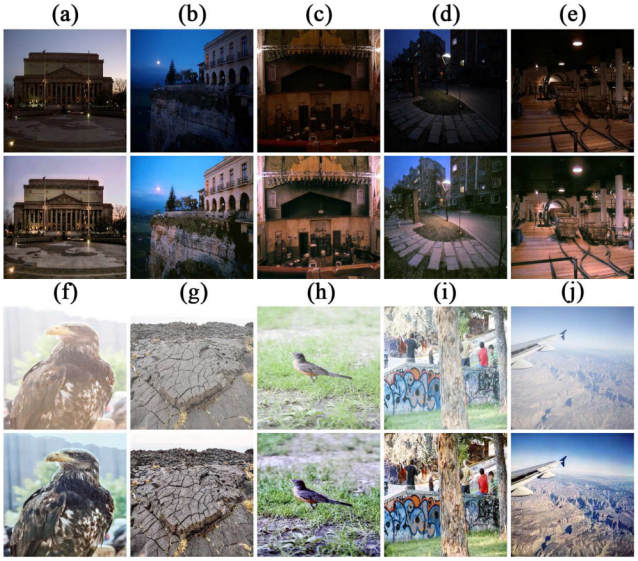

Figure 12: The application of the proposed method to low-light and overexposure scenes, where the first row of images are low-light images from the DICM and LIME datasets, the third row are overexposure images from the MIT-Adobe FiveK dataset, and the second and fourth rows are the enhanced images corresponding to our method.

5. Conclusion

In this paper, a dynamic supplement network based on cross aggregation transformer is proposed to enable significant quality enhancement of under-

water images. The overall framework consists of a shallow network and an enhancement network, where the enhancement network introduces a multi-scale enhancement process through an encoder/decoder structure. The shallow network uses multi-scale input information to extract shallow features. To enable more thorough enhancement of underwater images, we design a CAT to perform a channel-focused skip connection and utilize a RSM to focus on poorly enhanced regions and supplement detailed textures in real time. Experiments on public datasets demonstrate that the network enhances better with both CAT and RSM, not only significantly improving low-quality images in different scenes, but also having outstanding advantages in the comparison of many advanced methods. In further work, we will investigate the ability of the model on a wider range of enhancement tasks such as image denoising and image dehazing, and design more lightweight model to ensure the framework efficiency.

References

[1] T. P. Marques and A. B. Albu. L2uwe: A framework for the efficient enhancement of low-light underwater images using local contrast and multi-scale fusion, In Proceedings of the IEEE/CVF Conference on Computer Vision and Pattern Recognition, 2020, 538–539.

[2] G. Fan, Z. Hua, and J. Li. Multi-scale depth information fusion network for image dehazing, Applied Intelligence, 2021, 51(10): 7262–7280.

[3] Y. Yang, C. Wang, R. Liu, L. Zhang, X. Guo, and D. Tao. Self-augmented unpaired image dehazing via density and depth decomposition. In Proceedings of the IEEE/CVF Conference on Computer Vision and Pattern Recognition, 2022, 2037–2046.

[4] J. S. Jaffe. Computer modeling and the design of optimal underwater imaging systems[J]. IEEE Journal of Oceanic Engineering, 1990, 15(2): 101–111.

[5] B. McGlamery. A computer model for underwater camera systems. In Ocean Optics VI, 1980, 208: 221–231.

[6] C. Li, S. Anwar, J. Hou, R. Cong, C. Guo, and W. Ren. Underwater image enhancement via medium transmission-guided multi-color space embedding. IEEE Transactions on Image Processing, 2021, 30: 4985–5000.

[7] X. Ding, Y. Wang, Z. Liang, and X. Fu. A unified total variation method for underwater image enhancement. Knowledge-Based Systems, 2022, 255: 109751.

[8] Y. Wang, Y. Cao, J. Zhang, F. Wu and Z. Zha. Leveraging Deep Statistics for Underwater Image Enhancement. ACM Transactions on Multimedia Computing, Communications, and Applications, 2021, 17(3s): 1–20.

[9] H. Wang, P. Cao, J. Wang, and O. R. Zaiane. Uctransnet: rethinking the skip connections in u-net from a channel-wise perspective with transformer, In Proceedings of the AAAI Conference on Artificial Intelligence, 2022, 36(3): 2441–2449.

[10] C. O. Ancuti, C. Ancuti, C. De Vleeschouwer, and M. Sbert. Color channel compensation (3C): A fundamental pre-processing step for image enhancement. IEEE Transactions on Image Processing, 2019, 29: 2653–2665.

[11] M. Yang, A. Sowmya, Z. Wei, and B. Zheng. Offshore underwater image restoration using reflection-decomposition-based transmission map estimation. IEEE Journal of Oceanic Engineering, 2019, 45(2): 521–533.

[12] D. Berman, D. Levy, S. Avidan, and T. Treibitz. Underwater single image color restoration using haze-lines and a new quantitative dataset. IEEE Transactions on Pattern Analysis and Machine Intelligence, 2020, 43(8): 2822–2837.

[13] W. Song, Y. Wang, D. Huang, A. Liotta, and C. Perra. Enhancement of underwater images with statistical model of background light and optimization of transmission map. IEEE Transactions on Broadcasting, 2020, 66(1): 153–169.

[14] Y. Wang, C. Tang, M. Cai, J. Yin, S. Wang, L. Cheng, R. Wang, and M. Tan. Real-time underwater onboard vision sensing system for robotic gripping. IEEE Transactions on Instrumentation and Measurement, 2020, 70: 1–11.

[15] J. Zhou, T. Yang, W. Ren, D. Zhang, and W. Zhang. Underwater image restoration via depth map and illumination estimation based on a single image. Optics Express, 2021, 29(19): 29864–29886.

[16] Z. Liang, Y. Wang, X. Ding, et al. Single underwater image enhancement by attenuation map guided color correction and detail preserved dehazing. Neurocomputing, 2021, 425: 160–172.

[17] R. Miao, J. Qian, Y. Song, R. Ying, and P. Liu. UniVIO: Unified Direct and Feature-Based Underwater Stereo Visual-Inertial Odometry. IEEE Transactions on Instrumentation and Measurement, 2021, 71: 1–14.

[18] P. Zhuang, C. Li, and J. Wu. Bayesian retinex underwater image enhancement. Engineering Applications of Artificial Intelligence, 2021, 101: 104171.

[19] Z. Liang, X. Ding, Y. Wang, X. Yan, and X. Fu. Gudcp: Generalization of underwater dark channel prior for underwater image restoration. IEEE Transactions on Circuits and Systems for Video Technology, 2021, 32(7): 4879–4884.

[20] T. Li, S. Rong, W. Zhao, L. Chen, Y. Liu, H. Zhou, and B. He. Underwater image enhancement using adaptive color restoration and dehazing. Optics Express, 2022, 30(4): 6216–6235.

[21] J. Zhou, T. Yang, W. Chu, and W. Zhang. Underwater image restoration via backscatter pixel prior and color compensation. Engineering Applications of Artificial Intelligence, 2022, 111: 104785.

[22] X. Yan, G. Wang, G. Wang, Y. Wang, and X. Fu. A novel biologically-inspired method for underwater image enhancement. Signal Processing: Image Communication, 2022, 104: 116670.

[23] X. Li, C. Lei, H. Yu, and Y. Feng. Underwater image restoration by color compensation and color-line model. Signal Processing: Image Communication, 2022, 101: 116569.

[24] C. O. Ancuti, C. Ancuti, C. De Vleeschouwer, and P. Bekaert. Color balance and fusion for underwater image enhancement. IEEE Transactions on Image Processing, 2018, 27(1): 379–393. MR3729856

[25] K. Z. M. Azmi, A. S. A. Ghani, Z. M. Y usof, and Z. Ibrahim. Natural-based underwater image color enhancement through fusion of swarm-intelligence algorithm. Applied Soft Computing, 2019, 85: 105810.

[26] M. Awad, A. Elliethy, and H. A. Aly. Adaptive near-infrared and visible fusion for fast image enhancement. IEEE Transactions on Computational Imaging, 2019, 6: 408–418. MR3925193

[27] Z. Zhu, H. Wei, G. Hu, Y. Li, G. Qi, and N. Mazur. A novel fast single image dehazing algorithm based on artificial multiexposure image fusion. IEEE Transactions on Instrumentation and Measurement, 2020, 70: 1–23. MR4348363

[28] W. Zhang, L. Dong, T. Zhang, and W. Xu. Enhancing underwater image via color correction and bi-interval contrast enhancement. Signal Processing: Image Communication, 2021, 90: 116030.

[29] K. Liu and Y. Liang. Underwater image enhancement method based on adaptive attenuation-curve prior. Optics Express, 2021, 29(7): 10321–10345.

[30] J. Zhou, X. Wei, J. Shi, W. Chu, and W. Zhang. Underwater image enhancement method with light scattering characteristics. Computers and Electrical Engineering, 2022, 100: 107898.

[31] W. Zhang, Y. Wang, and C. Li. Underwater image enhancement by attenuated color channel correction and detail preserved contrast enhancement. IEEE Journal of Oceanic Engineering, 2022, 47(3): 718–735.

[32] L. Dong, W. Zhang, and W. Xu. Underwater image enhancement via integrated rgb and lab color models. Signal Processing: Image Communication, 2022, 104: 116684.

[33] J. Zhou, D. Zhang, and W. Zhang. Underwater image enhancement method via multi-feature prior fusion. Applied Intelligence, 2022: 1–23.

[34] X. Li, G. Hou, K. Li, and Z. Pan. Enhancing underwater image via adaptive color and contrast enhancement, and denoising. Engineering Applications of Artificial Intelligence, 2022, 111: 104759.

[35] W. Zhang, P. Zhuang, H.-H. Sun, G. Li, S. Kwong, and C. Li. Underwater image enhancement via minimal color loss and locally adaptive contrast enhancement. IEEE Transactions on Image Processing, 2022, 31: 3997–4010.

[36] Y. Huang, F. Yuan, F. Xiao, and E. Cheng. Underwater image enhancement based on color restoration and dual image wavelet fusion. Signal Processing: Image Communication, 2022, 107: 116797.

[37] C. Li, C. Guo, W. Ren, R. Cong, J. Hou, S. Kwong, and D. Tao. An underwater image enhancement benchmark dataset and beyond. IEEE Transactions on Image Processing. 2020, 29: 4376–4389.

[38] X. Fu and X. Cao. Underwater image enhancement with global–local networks and compressed-histogram equalization. Signal Processing: Image Communication, 2020, 86: 115892.

[39] Y. Wang, J. Guo, H. Gao, and H. Yue. UIEC2-Net: CNN-based underwater image enhancement using two color space. Signal Processing: Image Communication, 2021, 96: 116250.

[40] Z. Huang, J. Li, and Z. Hua. Underwater image enhancement via LBP-based attention residual network. IET Image Processing, 2022, 16(1): 158–175.

[41] Z. Fu, X. Lin, W. Wang, Y. Huang, and X. Ding. Underwater Image Enhancement via Learning Water Type Desensitized Representations, In IEEE International Conference on Acoustics, Speech and Signal Processing. 2022, 2764–2768.

[42] S. Liu, H. Fan, S. Lin, Q. Wang, N. Ding, and Y. Tang. Adaptive Learning Attention Network for Underwater Image Enhancement. IEEE Robotics and Automation Letters, 2022, 7(2): 5326–5333.

[43] Z. Huang, J. Li, Z. Hua, and L. Fan. Underwater Image Enhancement via Adaptive Group Attention-Based Multiscale Cascade Transformer. IEEE Transactions on Instrumentation and Measurement, 2022, 71: 1–18.

[44] J. Li, K. A. Skinner, R. M. Eustice, and M. Johnson-Roberson. WaterGAN: Unsupervised Generative Network to Enable Real-Time Color Correction of Monocular Underwater Images, In IEEE Robotics and Automation Letters, 2018, 3(1): 387–394.

[45] C. Fabbri, M. J. Islam, and J. Sattar. Enhancing underwater imagery using generative adversarial networks, In IEEE International Conference on Robotics and Automation. 2018, 7159–7165.

[46] X. Liu, Z. Gao, and B. M. Chen. MLFcGAN: Multilevel feature fusion-based conditional GAN for underwater image color correction. IEEE Geoscience and Remote Sensing Letters. 2019, 17(9): 1488–1492.

[47] Y. Guo, H. Li, and P. Zhuang. Underwater image enhancement using a multiscale dense generative adversarial network. IEEE Journal of Oceanic Engineering, 2019, 45(3): 862–870.

[48] L. Chen, Z. Jiang, L. Tong, Z. Liu, A. Zhao, Q. Zhang, J. Dong, and H. Zhou. Perceptual underwater image enhancement with deep learning and physical priors. IEEE Transactions on Circuits and Systems for Video Technology, 2020, 31(8): 3078–3092.

[49] M. J. Islam, Y. Xia, and J. Sattar. Fast underwater image enhancement for improved visual perception. IEEE Robotics and Automation Letters, 2020, 5(2): 3227–3234.

[50] C. Desai, R. A. Tabib, S. S. Reddy, U. Patil, and U. Mudenagudi. RUIG: Realistic Underwater Image Generation Towards Restoration, In Proceedings of the IEEE/CVF Conference on Computer Vision and Pattern Recognition, 2021, 2181–2189.

[51] Q. Jiang, Y. Zhang, F. Bao, X. Zhao, C. Zhang, and P. Liu. Two-step domain adaptation for underwater image enhancement. Pattern Recognition, 2022, 122: 108324.

[52] J. Hu, L. Shen and G. Sun. Squeeze-and-excitation networks. IEEE Transactions on Pattern Analysis and Machine Intelligence, 2020, 42(8): 2011–2023.

[53] Q. Wang, B. Wu, P. Zhu, P. Li, W. Zuo and Q. Hu, ECA-Net: Efficient Channel Attention for Deep Convolutional Neural Networks, In Proceedings of the IEEE/CVF Conference on Computer Vision and Pattern Recognition. 2020, 11531–11539.

[54] J. Deng, W. Dong, R. Socher, L.-J. Li, K. Li, and L. Fei-Fei. Imagenet: A large-scale hierarchical image database, In Proceedings of the IEEE/CVF Conference on Computer Vision and Pattern Recognition. 2009, 248–255.

[55] T. Ye, S. Chen, Y. Liu, Y. Ye, E. Chen, and Y. Li. Underwater Light Field Retention: Neural Rendering for Underwater Imaging, In Proceedings of the IEEE/CVF Conference on Computer Vision and Pattern Recognition. 2022, 488–497.

[56] M. J. Islam, P. Luo, and J. Sattar. Simultaneous enhancement and super-resolution of underwater imagery for improved visual perception. arXiv preprint arXiv:2002.01155, 2020.

[57] L. Zhang, L. Zhang, X. Mou, and D. Zhang. FSIM: A feature similarity index for image quality assessment. IEEE Transactions on Image Processing, 2011, 20(8): 2378–2386. MR2866342

[58] R. Zhang, P. Isola, A. A. Efros, E. Shechtman, and O. Wang. The unreasonable effectiveness of deep features as a perceptual metric, In Proceedings of the IEEE/CVF Conference on Computer Vision and Pattern Recognition. 2018, 586–595.

[59] M. Yang and A. Sowmya. An underwater color image quality evaluation metric. IEEE Transactions on Image Processing, 2015, 24(12): 6062–6071. MR3423828

[60] N. Yang, Q. Zhong, K. Li, R. Cong, Y. Zhao, and S. Kwong. A reference-free underwater image quality assessment metric in frequency domain. Signal Processing: Image Communication, 2021, 94: 116218.

[61] C. Lee, C. Lee and C. Kim, Contrast Enhancement Based on Layered

Difference Representation of 2D Histograms, IEEE Transactions on Image Processing, 2013, 22(12): 5372–5384.

[62] X. Guo, Y. Li, and H. Ling. Lime: Low-light image enhancement via illumination map estimation, IEEE Transactions on image processing, 2016, 26(2): 982–993. MR3604838

[63] V. Bychkovsky, S. Paris, E. Chan and F. Durand, Learning photographic global tonal adjustment with a database of input/output image pairs, In Proceedings of the IEEE/CVF Conference on Computer Vision and Pattern Recognition. 2011, 97–104.

Zhixiong Huang
School of Information and electronic engineering
Shandong Technology and Business University
Yantai 264005
China
E-mail address: hzxcyanwind@163.com

Jinjiang Li
School of Computer Science and Technology
Shandong Technology and Business University
Yantai
Shandong, 264005
China
E-mail address: lijinjiang@sdtbu.edu.cn

Zhen Hua
School of Information and electronic engineering
Shandong Technology and Business University
Yantai 264005
China
E-mail address: huazhen@sdtbu.edu.cn

Linwei Fan
School of Computer Science and Technology
Shandong University of Finance and Economics
Jinan, 250014
China
E-mail address: fanlinwei@sdufe.edu.cn

Received January 3, 2022